Do Nudging Tendencies Depend on the Nudging Timescale Chosen in Atmospheric Models?

[1,2]**Christopher G. Kruse,** [1]**Julio T. Bacmeister,** [3]**Colin M. Zarzycki,** [4,5]**Vincent E. Larson, and** [1]**Katherine Thayer-Calder**

[1]National Center for Atmospheric Research, Climate and Global Dynamics Laboratory, Boulder, Colorado
[2]NorthWest Research Associates, Boulder, Colorado
[3]Pennsylvania State University, Department of Meteorology and Atmospheric Science, University Park, Pennsylvania
[4]University of Wisconsin - Milwaukee, Department of Mathematical Sciences, Milwaukee, Wisconsin
[5]Pacific Northwest National Laboratory, Richland, Washington

Key Points:

- Nudging tendencies, or nudging forces per unit mass, depend strongly on the nudging time scale chosen (i.e. are $\propto \tau_{ndg}^{-1}$).
- Nudging tendencies cannot be *quantitatively* interpreted as errors in total (dynamics + physics) model forces on the atmospheric fluid
- Still, time-averaged differences between the modeled and target states can be useful in metrics for model evaluation.

Corresponding author: Christopher G. Kruse, ckruse@nwra.com

Abstract

Nudging is a ubiquitous capability of numerical weather and climate models that is widely used in a variety of applications (e.g. crude data assimilation, "intelligent" interpolation between analysis times, constraining flow in tracer advection/diffusion simulations). Here, the focus is on the momentum nudging tendencies themselves, rather than the atmospheric state that results from application of the method. The initial intent was to interpret these tendencies as a quantitative estimation of model error (net parameterization error in particular). However, it was found that nudging tendencies depend strongly on the nudging time scale chosen, which is the primary result presented here. Reducing the nudging time scale reduces the difference between the model state and the target state, but much less so than the reduction in the nudging time scale, resulting in increased nudging tendencies. The dynamical core, in particular, appears to increasingly oppose nudging tendencies as the nudging time scale is reduced. These results suggest nudging tendencies cannot be *quantitatively* interpreted as model error. Still, nudging tendencies do contain some information on model errors and/or missing physical processes and still might be useful in model development and tuning, even if only qualitatively.

Plain Language Summary

Nudging is a common feature of weather and climate models used to guide the model's atmospheric state along the observed atmospheric evolution in the past. Here, an initial attempt was made to interpret the nudging tendencies as model error. However, it was learned that these nudging tendencies change when the nudging time scale is changed, largely due to the model's dynamical core opposing the effect of the nudging in trying to achieve its desired state. Results presented here suggest the model wins this "tug-of-war." The overall conclusions is that these nudging tendencies cannot be quantitatively interpreted as model error, but still have some use in identifying model issues, even if only qualitatively.

1 Introduction

Nudging atmospheric models is a process where a linear relaxation term is introduced into the governing equation for some variable (e.g. the zonal wind, u). The nudging term produces a tendency that acts to bring that variable toward some target state. For example, the prognostic equation for u can be written

$$\frac{\partial u}{\partial t} = D_x(\boldsymbol{\phi}) + P_x(\boldsymbol{\phi}) + N_x(u, u_0), \tag{1}$$

where $D_x(\,.\,)$ is the sum of zonal wind tendencies from dynamical terms (e.g. advection, pressure gradient, Coriolis), $P_x(\,.\,)$ is the sum of zonal wind tendencies from physical parameterizations (turbulence, gravity wave drag, ...), $\boldsymbol{\phi}$ a vector of variables making up the state required by dynamics and physics model components, and $N_x(u, u_0)$ is the added linear relaxation nudging term defined below.

The form of nudging term, $N_x(u, u_0)$, depends on the type of target state, u_0. For example, the target state might be a particular observation, with nudging tendencies proportional to the difference between the model state and the observation, inversely proportional to distance in space and time, and inversely proportional to some specified nudging time scale, τ_{ndg}. This approach is referred to as observational nudging. Another possibility is that the target state is a gridded analysis, referred to as analysis nudging. In this case, the nudging term often takes the following form:

$$N_x(u, u_0) = -W\left(\frac{u - u_0}{\tau_{ndg}}\right) \tag{2}$$

where $u_0 = u_0(x, y, z, t)$ is some target state (e.g. analysis) spatiotemporally interpolated onto the host model grid and $W = W(x, y, z, t)$ is a weighting function that can be used to limit nudging to certain regions, model levels, or times. Here, analysis nudging is the focus with the weighting function set to unity ($W = 1$).

The use of such nudging first appears in scientific literature in the mid-1970s (Kistler, 1974; Anthes, 1974; Davies & Turner, 1977). The original application was to use nudging to assimilate data for analyses and model initial conditions. This approach more continuously assimilated information from data, preventing numerical instabilities that arose in previous assimilation methods that simply inserted observations (e.g. Charney et al. (1969); Jastrow and Halem (1970)). For additional early historical context and applications, see Stauffer and Seaman (1990) and Skamarock et al. (2008).

Subsequently, another application of analysis nudging was first demonstrated in Kao and Yamada (1988), where a numerical weather model was nudged to analyzed observations, allowing realistic tracer transport and diffusion with synoptic-scale meteorology constrained. Such an exercise was sometimes preferable to just using the standard 12-hourly analyses of the time, allowing physical processes represented in the model to influence the state trajectory and tracer advection/diffusion between analyses in a plausible way. Currently, using analysis nudging to constrain meteorology in advection, diffusion, and chemistry models is fairly common, often referred to as a "specified dynamics" configuration of some host model (e.g. Davis et al. (2021)).

Here, the initial intent was to use nudging to approximate errors in model parameterizations, with particular interest in errors in the momentum equations. As nudging keeps the host model's state close to a presumably accurate target state, one might interpret the nudging tendencies time averaged over, say, a season, to to be the net error in total (i.e. dynamical core + all parameterization tendencies) model forcing per unit mass (Eq. 1). If one were to further assume dynamical core errors are significantly smaller than those introduced by the physical parameterizations and the target state is accurate, then the nudging tendencies might be interpreted more specifically as the net error of all parameterizations. Then, nudging tendencies and physical understanding of relevant processes at play could be used to attribute errors to particular processes and these errors might be quantitatively targeted. Mapes and Bacmeister (2012) use similar arguments to interpret incremental analysis update tendencies as net error of all physics parameterizations.

However, while evaluating such an approach, it was found that nudging tendencies are proportional to the inverse of the nudging time scale (τ_{ndg}^{-1}) chosen and, therefore, cannot be interpreted as total model (dynamics + physics) error or net physics error, at least not *quantitatively*. The sole objective of this article is to present this apparently unpublished, if not completely unknown, result. The ubiquity of nudging capabilities and their many, frequent uses within weather and climate models motivate presentation of this result.

Here, nudging tendencies required to keep the Community Atmosphere Model, version 6 (CAM6, Gettelman et al. (2019)), close to the ERA5 reanalysis (Hersbach et al., 2020) over five recent winters are analyzed, with nudging time scales varied from 3 to 24 hours. The model configuration and experiments are described in Section 2. The primary result that nudging tendencies are proportional to τ_{ndg}^{-1} is presented in Section 3. In Section 4, a heuristic theoretical argument for this result is provided. A summary and discussion of the results is given in Section 5.

2 Model Configuration and Experiment Design

The default CAM6 was used to simulate five winters from 2008 to 2012 with specified sea surface temperatures and sea ice (i.e. the "FHIST" component set was specified) on a ≈1 degree latitude/longitude grid with the finite-volume dynamical core. The model was initialized every 1 Dec with ERA5 interpolated onto its grid and integrated for three months (i.e. over December, January, and February (DJF)). During the integrations, CAM was continuously nudged to ERA5 winds, temperatures, and humidities at every time step. With a time step of 30 minutes, the target state, $\boldsymbol{\phi}_0 = (u_0, v_0, T_0, q_0)$, was updated to ERA5 at the top of every hour and to ERA5 linearly interpolated in time half-past every hour. Four such simulations of these five winters were completed, each with a constant nudging time scale of $\tau_{ndg} = 3$, 6, 12, and 24 hours.

All tendencies acting on the zonal and meridional winds were output. Exact budget closure was verified. Here, generally, the net tendencies by the dynamical core and by all physical parameterizations are presented, often referred to as "dynamics" and "physics" tendencies. Figure 1 shows the DJF-averaged net dynamics, physics, and nudging tendencies projected along the DJF-averaged wind horizontal wind vector vertically averaged over the lowest four levels. For example, the nudging tendencies in Fig. 1d were computed via

$$\overline{N} = \frac{\int \langle \mathbf{N} \rangle \cdot \widehat{\langle \mathbf{u} \rangle} \langle \rho \rangle \, dz}{\int \langle \rho \rangle \, dz}. \tag{3}$$

where $\langle \, . \, \rangle$ is a DJF, 2008-2012 time average and $\widehat{\langle \mathbf{u} \rangle}$ is a unit vector pointing in the direction of of the DJF, 2008-2012 time averaged horizontal wind vectors.

2.1 Typical DJF Momentum Balances

Here, the focus is on the lowest four model levels, as an initial interest was low-level wind biases that nudging tendencies at these levels highlight. Generally, the dynamical core acts to accelerate the low-level flow (Fig. 1a), while the physical parameterizations (the turbulence and low-level drag parameterizations in particular) oppose these dynamics tendencies and act to decelerate the low-level flow (Fig. 1b). The dynamics and physics tendencies do not exactly cancel, however (Fig. 1c). The residual of these two tendencies is almost exactly compensated by the nudging tendencies. This is expected, as $\partial_t \mathbf{u} \approx \mathbf{0}$ after time averaging over DJF, requiring the sum of the dynamics/physics residual tendencies and the nudging tendencies to be small as well (Eq. 1). The total wind time-averaged tendencies are an order of magnitude smaller than those in the bottom row of Fig. 1 (not shown).

3 Do Nudging Tendencies Change with τ_n?

To get a sense for how robust nudging-tendency-derived model error estimates were, nudging time scales were varied while keeping the model configuration (default except for the nudging) unchanged. The momentum nudging tendencies, $\overline{N}$, are shown in Fig. 2 for four runs with τ_{ndg} varied from 3 to 24 hours.

Two results are immediately apparent: the spatial structure of the momentum nudging tendencies are quite consistent across the four runs and the nudging tendencies increase with decreasing τ_{ndg}. These results held when looking at the middle troposphere and lower stratosphere as well (not shown). Nudging tendencies tend to exert additional drag over regions with significant topography (e.g. the Andes, the Rocky Mountains, the Himalayas, the flanks of Antarctica) in all four simulations. These tendencies also exert drag on the low-level winds in all four runs over the Southern Ocean, with tenden-

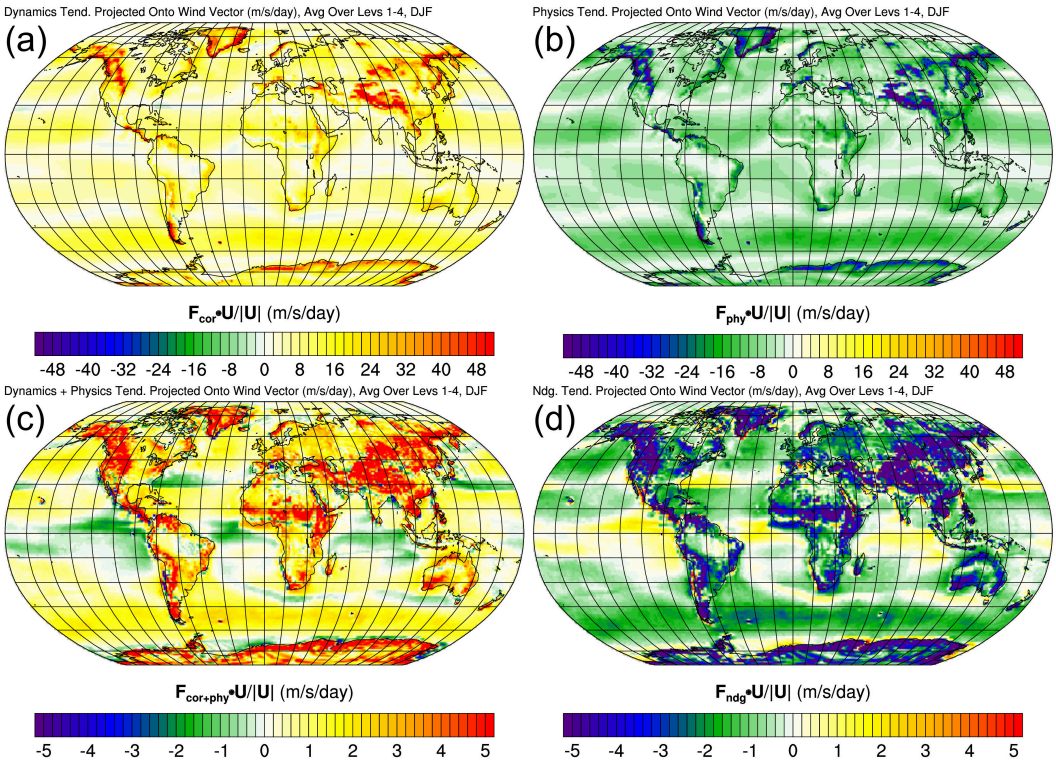

Figure 1. DJF-, 2008-2012-averaged horizontal momentum budget components projected along the similarly averaged horizontal wind and vertically averaged over the lowest four model levels, computed via Eq. 3, are color shaded. The net dynamics tendencies ($\overline{D}$) and net physics tendencies ($\overline{P}$) are shown in (a) and (b). The sum of dynamics and physics ($\overline{D} + \overline{P}$) are shown in (c). Nudging tendencies ($\overline{N}$) are shown in (d). Note the different order of magnitude in the color bars in each row.

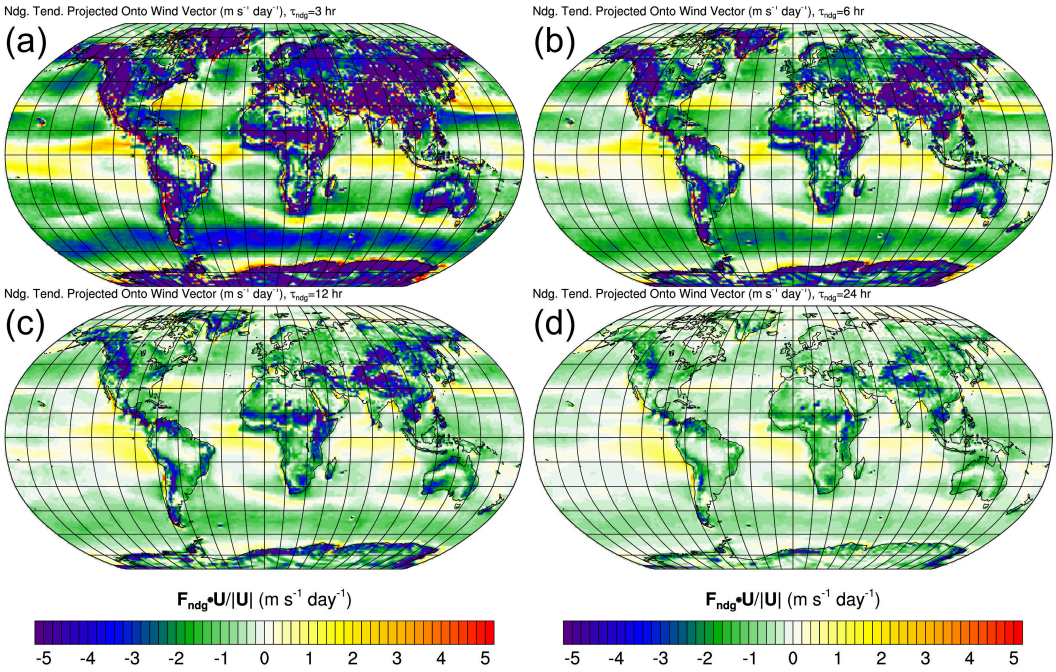

Figure 2. DJF-, 2008-2012-averaged horizontal momentum nudging tendencies projected along the similarly averaged horizontal wind and vertically averaged over the lowest four model levels are color shaded. The four panels show maps of these nudging tendencies from four runs with nudging time scales of (a) 3 hours, (b) 6 hours, (c) 12 hours, and (d) 24 hours.

cies somewhat invariant in longitude at these latitudes. Regions where the model might be exerting too much drag and the nudging tendencies tend to accelerate the low-level flow also display some consistency across the runs, though, perhaps less so than the regions of inferred too little drag.

Scatter plots of time-averaged zonal dynamics, physics, and momentum nudging tendencies at individual grid points on the lowest four model levels from one run plotted versus corresponding tendencies from the run with twice the nudging time scale are shown in Fig. 3. Best fit linear regressions and r^2 values shown in each panel. Nudging tendencies at individual grid points are consistent between runs with τ_{ndg} changed by a factor of two, indicated by the fairly linear relation between the nudging tendencies and the high r^2 (≥ 0.911) values. Slopes of the linear regressions are significantly larger than one, though, a bit less than the expected slope of 2 if nudging tendencies were exactly proportional to the inverse nudging time scale. However, these regressions are influenced by a majority of points with small tendencies. Grid points with the largest tendencies do track more closely to a 2-to-1 line. Regardless, the nudging tendencies are roughly proportional to τ_{ndg}^{-1} over τ_{ndg} ranging from 3 to 24 hours even grid-point by grid-point. The dynamics and physics tendencies are much more consistent when τ_{ndg} is changed by a factor of 2, falling much closer to a 1-to-1 line.

Similar maps and scatter plots of temperature nudging tendencies are shown in Figs. 4 and 5. Temperature nudging tendencies have a similar dependence on τ_{ndg}, with tendencies also increasing with decreasing τ_{ndg}. However, this dependence is less strong than that with the momentum nudging tendencies (c.f. Figs. 3 and 5 a-c).

If nudging tendencies were to give a robust/consistent estimate of model error of a model in a particular configuration, one might expect that the difference between the

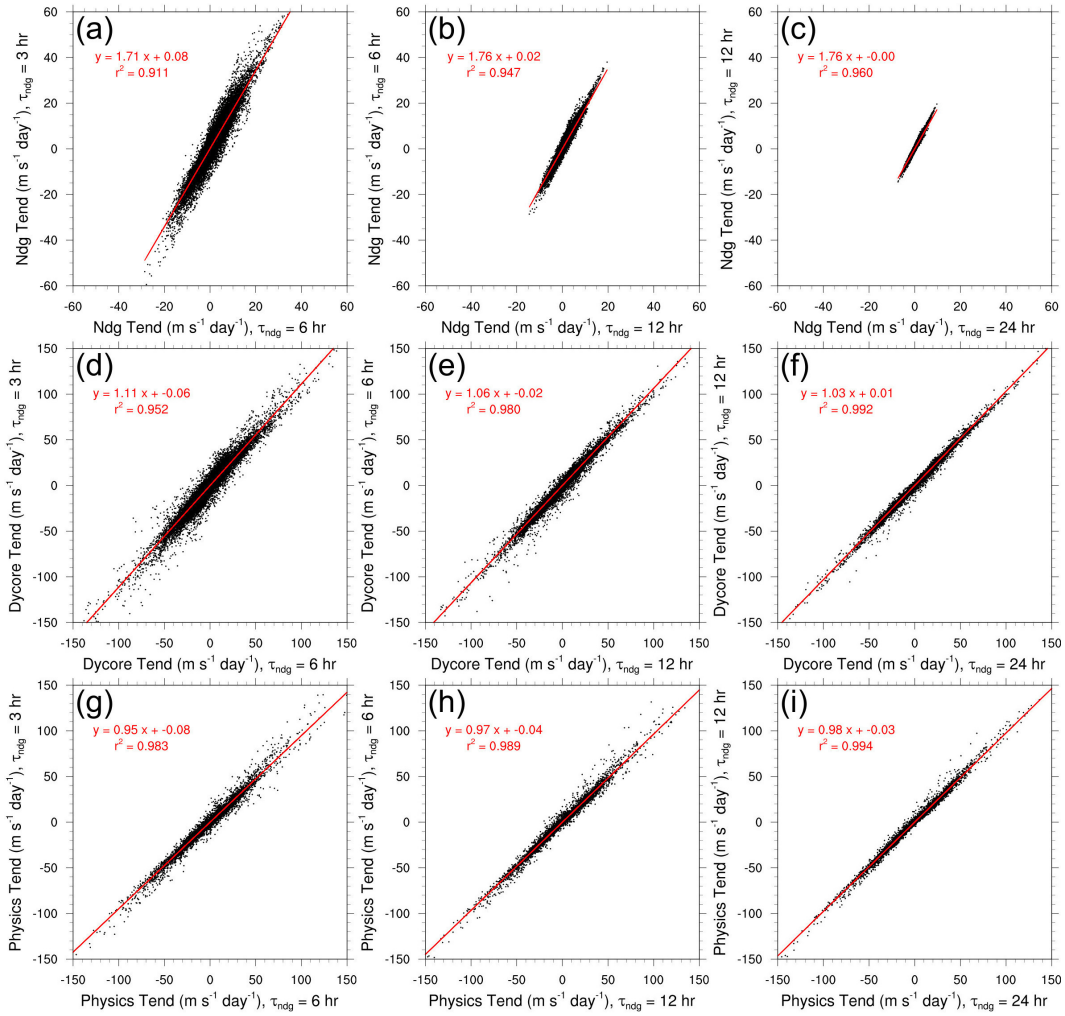

Figure 3. Scatter plots of (top) nudging, (middle) dynamical core, and (bottom) physics tendencies from a nudging run plotted versus the same quantities from a run with twice the nudging time scale. Each point represents the DJF, 5-season time averaged tendency on a grid point on one of the four lowest model levels. Runs with nudging time scales of 3, 6, 12, and 24 hours were used. Best fit lines and corresponding r^2 values are overlaid in red.

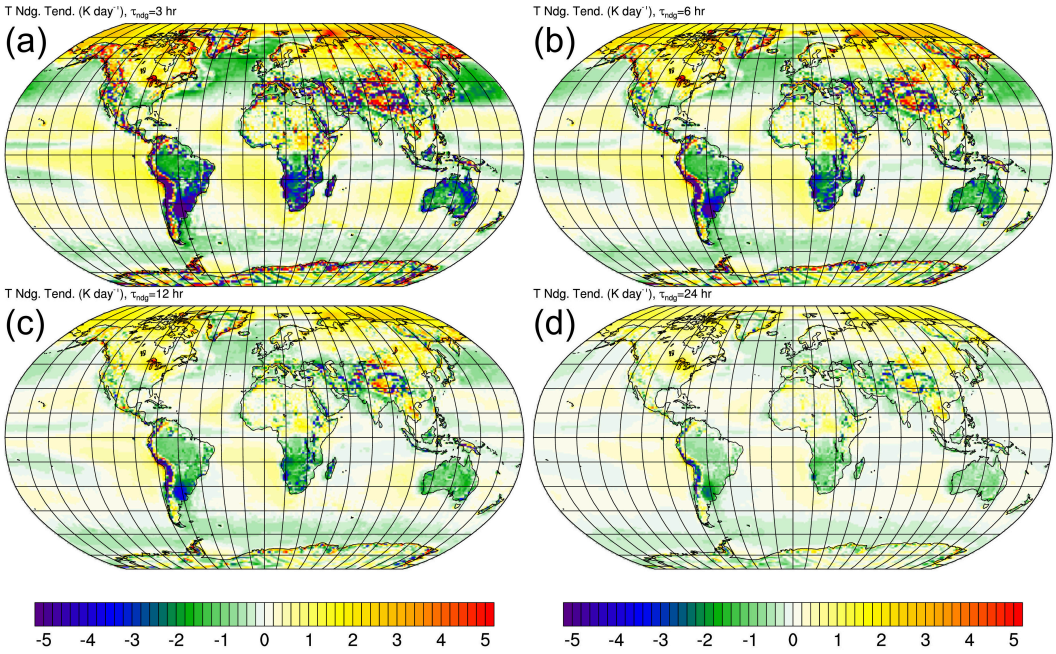

Figure 4. DJF-, 2008-2012-averaged temperature nudging tendencies vertically averaged over the lowest four model levels are shown in color shading. The four panels show maps of these nudging tendencies from four runs with nudging time scales of (a) 3 hours, (b) 6 hours, (c) 12 hours, and (d) 24 hours.

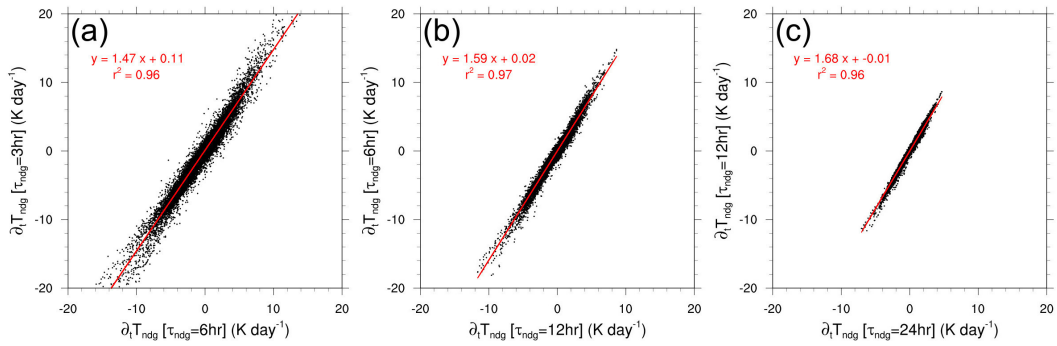

Figure 5. Scatter plots of temperature nudging tendencies from a nudging run plotted versus the same quantities from a run with twice the nudging time scale. Each point represents the DJF, 5-season time averaged tendency on a grid point on one of the four lowest model levels. Runs with nudging time scales of 3, 6, 12, and 24 hours were used. Best fit lines and corresponding r^2 values are overlaid in red.

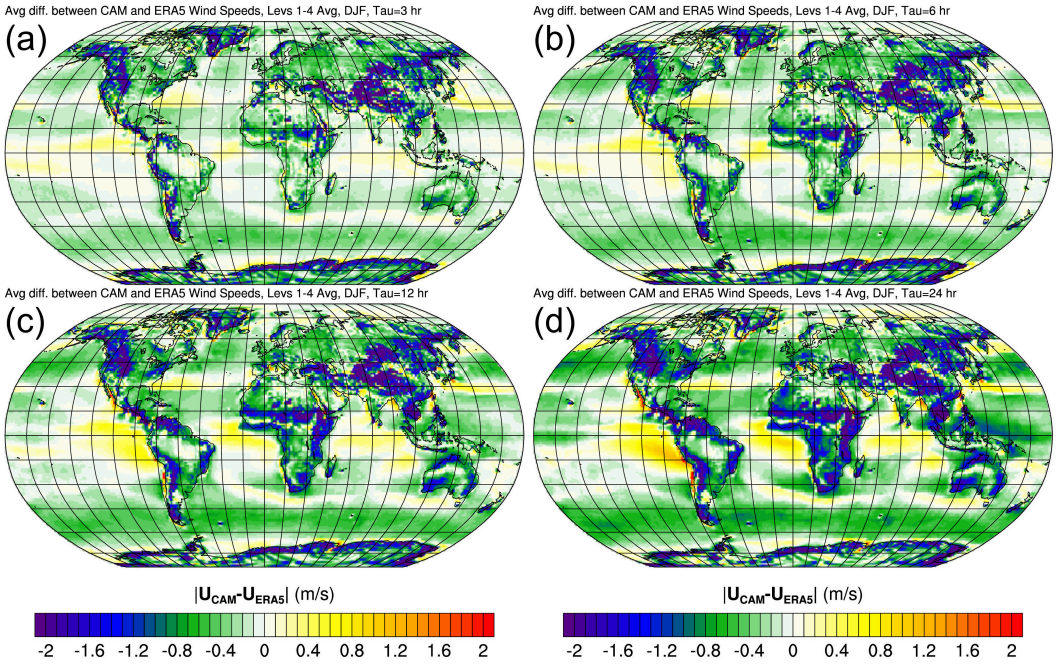

Figure 6. Same as Fig. 2, but with each panel multiplied by its corresponding nudging time scale. This gives the time-average, level-1-4-average, difference in wind speed between CAM and ERA5.

	3 hr vs 6 hr	6 hr vs 12 hr	12 hr vs 24 hr
Slope	0.87	0.89	0.89
Offset	0.01	0.01	0.00
r^2	0.92	0.95	0.96

Table 1. Linear regression coefficients and r^2 values from scatter plots of $\tau_{ndg,1}\langle\mathbf{N}\rangle\cdot\widehat{\langle\mathbf{u}\rangle}$ plotted vs $\tau_{ndg,2}\langle\mathbf{N}\rangle\cdot\widehat{\langle\mathbf{u}\rangle}$, where $\tau_{ndg,1}=0.5\tau_{ndg,2}$. These differences on the lowest four model levels were used, without the vertical averaging applied in Fig. 6, Eq. 3. Scatter plots not shown.

model state and the target state (i.e. the numerator in Eq. 2) to reduce proportionately to the reduction in nudging time scale. Given that nudging tendencies increase, the difference between the model state and the target state is not being reduced proportionately. The DJF-2008-2012-, level-1-4-averaged momentum nudging tendencies, $\overline{N}$, in Fig. 2 are multiplied by the τ_{ndg} used in each run to illustrate how the time-averaged difference between the model and target state varies in Fig. 6. Decreasing the nudging time scale by a 50% does bring the model state closer to the target state, but only by $\approx 12\%$ (Table 1).

Because nudging does keep the model state close to the target state (Fig. 6) and the DJF-2008-2012-average total wind tendencies are an order of magnitude smaller than the nudging tendencies in all runs ($\partial_t\mathbf{u}\approx 0$, not shown), the momentum budget (e.g. Eq. 1) requires a compensation in model tendencies somewhere. This is hinted at by the anti-correlation of the net model tendencies and nudging tendencies in the bottom row of Fig. 1, consistent with Bao and Errico (1997) (their Section 4). The changes in dynamics and physics tendencies are plotted versus the changes in nudging tendencies on grid points in Fig. 7 for runs with τ_{ndg} changed by a factor of two. Interestingly, this com-

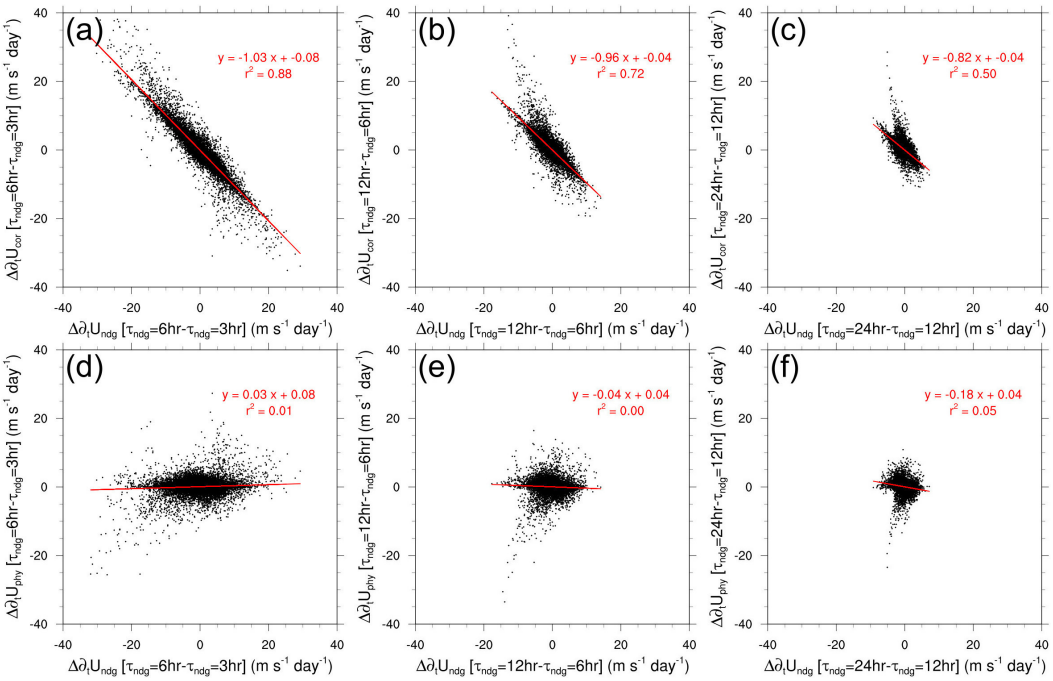

Figure 7. Scatter plots of changes of (top) dynamical core tendencies and (bottom) physics tendencies plotted versus changes in nudging tendencies when reducing nudging time scales by a factor of two. Each point represents such differences in DJF, 5-season averaged tendencies at grids points on one of the lowest four model levels.

pensation occurs primarily in dynamics tendencies, being particularly clear at the smaller nudging time scales.

These results suggest that, at least when the model configuration is not changed, the physical processes represented by the dynamical core are primarily responsible for compensating these nudging tendencies. In other words, the dynamical core is responsible for fighting the effect of the nudging and reducing the ability of the nudging term to bring the model state closer to the target state. A heuristic theoretical representation of the nudged model system is presented in the following section to speculate on how the dynamical core is fighting the nudging tendencies and why these tendencies are proportional to the inverse nudging time scale.

4 Time Scale Analysis

Some progress can be made in understanding why nudging tendencies vary with τ^{-1} using a simple time scale analysis. Here, the entire host model (i.e. $D_x(\boldsymbol{\phi})+P_x(\boldsymbol{\phi})$) is heuristically represented by a linear relaxation term:

$$\frac{\partial u}{\partial t} \approx -\frac{u-u_{mod}}{\tau_{mod}} - \frac{u-u_0}{\tau_{ndg}} \tag{4}$$

where u_{mod} is some zonal wind the model is trying to achieve on some model timescale, τ_{mod}. A target state for the whole nudged system (u_s) and system relaxation time scale (τ_s) are defined as

$$\tau_s = \frac{\tau_{ndg}\tau_{mod}}{\tau_{ndg} + \tau_{mod}}, \tag{5}$$

and

$$\frac{u_s}{\tau_s} = \frac{u_{mod}}{\tau_{mod}} + \frac{u_0}{\tau_{ndg}}. \tag{6}$$

With these definitions, the state of the nudged model system can be expressed as a weighted average of the nudging and model time scales:

$$u_s = \frac{\tau_{ndg}}{\tau_{ndg} + \tau_{mod}} u_{mod} + \frac{\tau_{mod}}{\tau_{ndg} + \tau_{mod}} u_0. \tag{7}$$

Correspondingly, the momentum equation can be written as

$$\frac{\partial u}{\partial t} \approx -\frac{u - u_s}{\tau_s}. \tag{8}$$

In this simple system, the model is trying to achieve its desired state (i.e. the model is pulling the nudged system state toward its attractor, $u_{mod}(x, y, z, t)$) while the nudging term is trying to pull the nudged model's state to the target state ($u_0(x, y, z, t)$, Eq. 4). Alternatively, the nudged model state is essentially being relaxed to a timescale-weighted average of the target and model attractor states on the system timescale (Eq. 8).

Eq. 8 implies that, averaged over sufficient time, the time-averaged nudged model state should just be the time-averaged system state:

$$\langle u \rangle^t = \langle u_s \rangle^t. \tag{9}$$

where $\langle\, . \,\rangle^t$ is a time-average operator. The time-averaged nudging tendencies were presented in the previous section. The following expression for the time-averaged nudging tendencies follows from Eqs. 2, 7, and 9:

$$\langle N_x \rangle^t = -\frac{\langle u \rangle^t - \langle u_0 \rangle^t}{\tau_{ndg}} = -\frac{\langle u_{mod} \rangle^t - \langle u_0 \rangle^t}{\tau_{mod} + \tau_{ndg}} \tag{10}$$

This relation suggests that as long as the state the host model is trying to achieve (i.e. its attractor, $\langle u_{mod} \rangle^t$) differs from the target state ($\langle u_0 \rangle^t$) systematically, there will be non-zero time-averaged nudging tendencies. The magnitude of these nudging tendencies depends on how different the state the host model is trying to achieve and the target state are. The model and nudging time scales also play a role. However, if the model time scale is sufficiently small relative to the nudging time scale ($\tau_{mod} << \tau_{ndg}$), or it is somehow dictated by the imposed nudging time scale (i.e. $\tau_{mod} \propto \tau_{ndg}$), then the time averaged nudging tendencies will be proportional to the inverse of the nudging time scale, consistent with the model result presented above. The model time scale is further discussed and estimated from the model output below.

4.1 Model Time Scales

What is this model time scale and what values might it have? Nudging tendencies likely act to bring the model away from its desired state, while the model (i.e. the dynamical core in particular) tends to oppose these tendencies as it tries to achieve its desired state. Here, it is speculated that the model relaxation term in Eq. 4 represents the host model's adjustment to imbalances produced by dynamical, physical or nudging tendencies. A classical, albeit idealized, example of a fluid adjusting from an imbalanced state to a balanced one is geostrophic adjustment (Blumen, 1972). In the geostrophic

adjustment problem, the time scale of adjustment is usually treated as an order of magnitude smaller than the time scale of evolution of a fluid in geostrophic balance. In absolute terms, geostrophic adjustment occurs over a time scale of an inertial period ($2\pi/f$, where f is the Coriolis parameter), which depends on latitude, but has values of 12 hours at the poles that increase toward the equator. In reality, and within numerical models, excess momentum associated with a variety of physical imbalances (e.g. deviations from cyclo-geostrophic balance, quasi-geostrophic balance, semi-geostrophic balance, non-linear balance) is shed via generation of, and transport by, atmospheric waves (e.g. gravity waves (GWs), inertia gravity waves, Kelvin waves, (Plougonven & Zhang, 2014)). Outside of the tropics, GWs are emitted from these imbalances, having time scales ranging from the buoyancy period ($\approx$ 10 minutes) to the inertial period ($\approx$ 10 hours). If the time scale of adjustment to the imbalances produced by the nudging tendencies is similar to the time scales of the waves generated by the adjustment process, then τ_{mod} would likely be in the range of 10 minutes to 10 hours. This range of τ_{mod} ($10\,min \lesssim \tau_{mod} \lesssim 10\,hrs$) is a bit smaller than the range of τ_{ndg} ($3\,hrs \leq \tau_{ndg} \leq 24\,hrs$) used here, and so might be consistent with argument above that nudging tendencies are proportional to τ_{ndg}^{-1} because $\tau_{mod} << \tau_{ndg}$.

Here, the model relaxation time scales were estimated from the 3-hourly-averaged momentum tendencies by regressing the model tendencies (i.e. D_x+P_x) versus the difference between the 3-hourly-averaged nudged-system and model attractor states, $u - u_{mod}$. This difference is not known because u_{mod} is not known. However, if the differences between the time-varying target state and the model's desired state are much smaller than the time-varying differences of the nudged model system state from the model's desired state or the target state,

$$|(u - u_{mod}) - (u - u_0)| = |u_0 - u_{mod}| << |u - u_{mod}|, |u - u_0|,$$

then $u - u_{mod}$ can be approximated by $u - u_0$, which can be easily computed from the nudging tendencies multiplied by the corresponding τ_{ndg}. The model tendencies were regressed against $u - u_0$ at every grid point on the 4th model level, and the model time scales were then computed from the inverse of the regression slopes. These estimates of τ_{mod} are shown in Fig. 8 in both absolute units and relative to the nudging time scale used. Regions color shaded are those where the probability the regression slope is non-zero is greater than 99%. An additional consistency check on this approach is provided by the correlation coefficients between $D_x + P_x$ and $u - u_{mod}$ (not shown). Correlations are modest but generally significant, with values in the range of -0.5 to -0.75 in parts of the Southern Ocean and Subtropics.

The magnitude of the τ_{mod} estimate is quite variable across the globe (left column of Fig. 8). This might not be so surprising, as time scales of geostrophic adjustment and maximum time scales of GWs that can be emitted both decrease with increasing distance from the equator. Zonal asymmetry in τ_{mod} is also quite apparent, both due to significantly smaller τ_{mod} over land vs ocean and zonal variability over just ocean as well. Regions of larger τ_{mod} occur in regions with small nudging tendencies and at low latitudes.

The heuristic analysis above suggested that if τ_{mod} is significantly smaller than τ_{ndg}, or proportional to τ_{ndg}, then the time-averaged nudging tendencies could be expected to be proportional to τ_{ndg}^{-1}. Over the Southern Ocean where additional drag is being exerted in all nudging runs, both seem to be true to an extent. The τ_{mod} estimates increase with increasing τ_{ndg}, but less so than expected if τ_{mod} were truly proportional to τ_{ndg}. This is perhaps better seen in the maps of τ_{mod}/τ_{ndg} in Fig. 8e-f. The ratio τ_{mod}/τ_{ndg} decreases as τ_{ndg} is increased from about 1/2 when $\tau_{ndg} = 3$ hrs to about 1/3 when $\tau_{ndg} =$ 24 hrs.

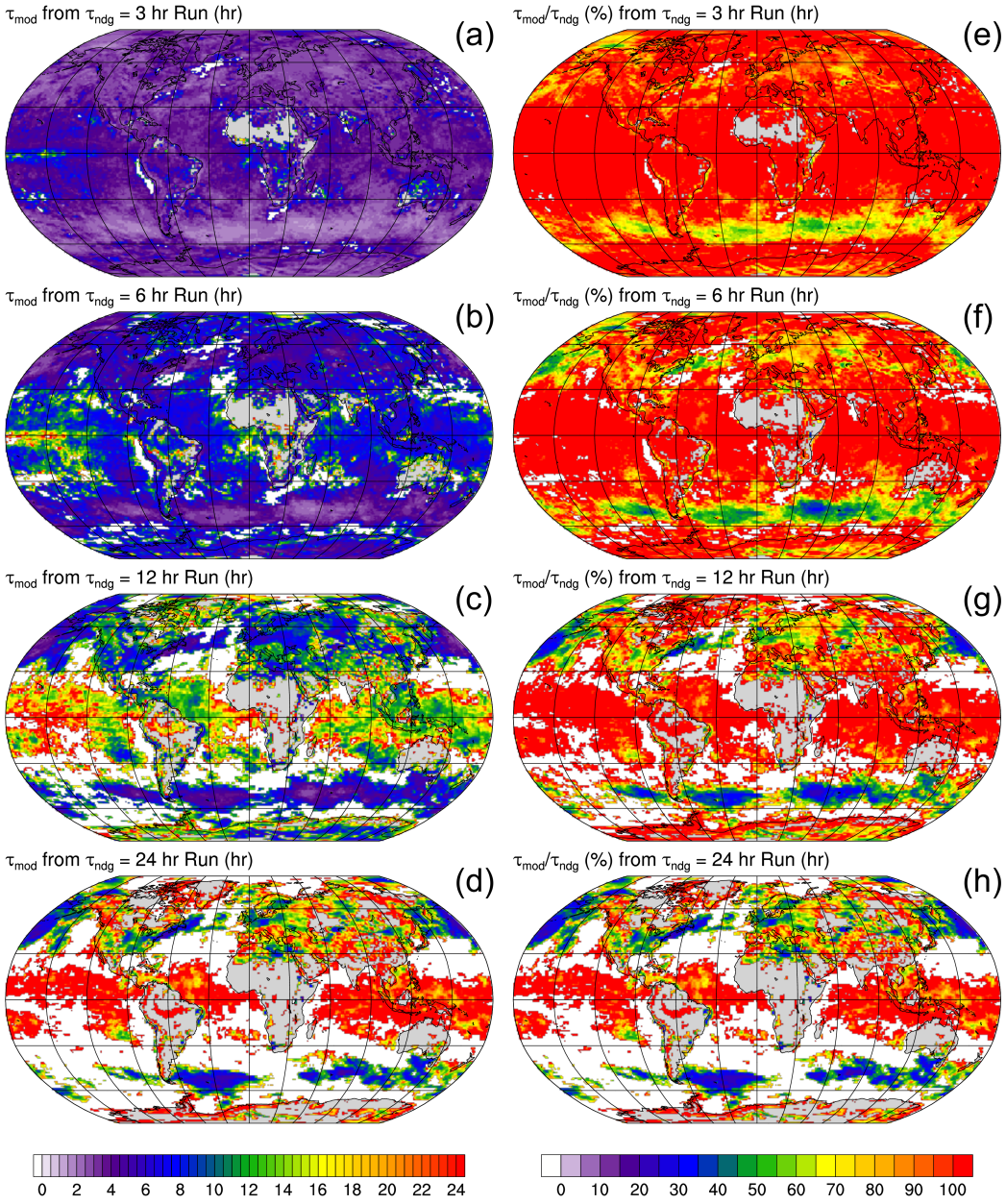

Figure 8. Maps of τ_{mod} estimated by regressing 3-hr-average $D_x + P_x$ vs $u - u_0$ during the 2008-2009 DJF at each grid point on the fourth model level. Both (left) τ_m [hr] and (right) τ_m/τ_n [%] are shown. Only regions where the regression slope is statistically significant at the 99% confidence level are shown.

All this is to say that the model is quite effective at opposing nudging tendencies, in part because the model (the dynamical core in particular) can adjust significantly faster (50%-70%) than the nudging term can pull the nudged model state toward the target state. Interestingly, the model's adjustment time scales also appear to be dictated, to some extent, by the chosen nudging time scale. How the model's dynamical core increasingly opposes the increasing nudging tendencies is interesting. Perhaps the dynamical core makes more efficient use of/uses more adjustment mechanisms/instabilities at its disposal to increasingly oppose nudging tendencies' pull away from its desired state. The model's response to the nudging tendencies was not investigated further here.

5 Can Nudging Tendencies Identify Missing/Erroneous Processes?

Everything presented thus far was based on CAM simulations with the same configuration, but with nudging time scales varied. However, a more practical use of the nudging method might be to change the model configuration (e.g. parameterizations), perhaps as part of a model development or tuning process, and use the nudging tendencies to evaluate whether or not the fast model processes have been improved. While it's clear nudging tendencies cannot be *quantitatively* interpreted as the net forcing error of the model or all its parameterizations because these tendencies depend strongly on the chosen nudging time scale, nudging tendencies can still point out problem regions qualitatively. Here, nudging tendencies from two CAM runs, one with the Beljaars low-level orographic drag parameterization and one without, nudged to ERA5 are briefly compared. This parameterization was chosen as it exerts very strong forces on the low-level flow and has an easily recognisable spatial distribution (i.e. it mainly acts over significant mountain ranges).

Figure 9 shows the absolute value of changes in DJF-2008-2012-averaged nudging, Beljaars, dynamics, and physics tendencies between the two runs. Encouragingly, when this parameterization is removed, nudging tendencies act to replace these parameterized tendencies (cf. Figs. 9a and b). However, the low-level drag added by the nudging to replace this process is only $\approx$25% of the tendencies by this process in the run with it enabled. This result further suggests, while nudging tendencies can useful in identifying model errors and/or missing processes, they can only be used qualitatively.

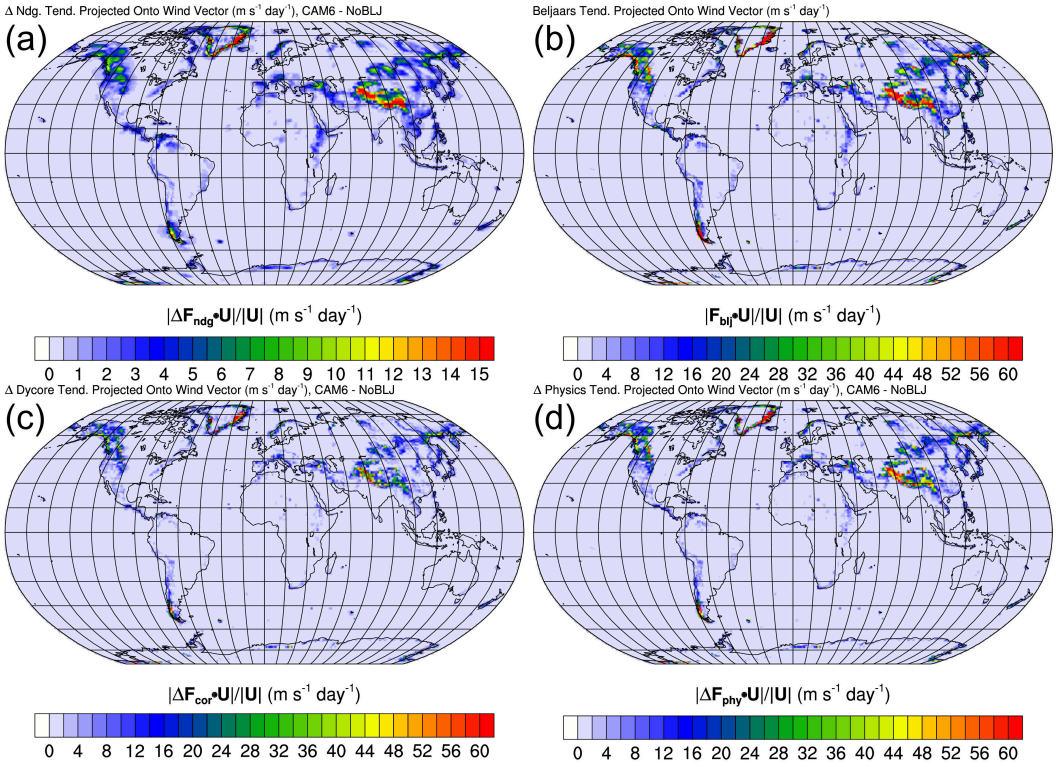

Figure 9. Absolute changes in zonal wind tendencies between runs with (CAM6) and without (NoBLJ) the Beljaars turbulent orographic form drag parameterization vertically averaged over the four lowest model levels. (a) Change in zonal wind nudging tendencies. (b) The Beljaars drag tendency. (c) The change in zonal wind dynamics tendencies. (d) The change in the total physics tendency.

6 Summary

The primary result of this article is that nudging tendencies that result from nudging a model to a target state are proportional to the inverse of the nudging time scale chosen (Figs. 2, 3a-c). As momentum nudging tendencies increase, they are increasingly compensated by changes in tendencies by the dynamical core (Fig. 7, top row), presumably to adjust to imbalances introduced by the nudging. A heuristic time scale analysis suggests that if the model's imbalance adjustment time scale is significantly smaller than, or proportional to, the chosen nudging time scales, this result should be expected as long as the target state to which the model is being nudged is different from the state the model is trying to achieve, regardless of the type of target state (e.g. a native analysis, a non-native analysis, some other model entirely that has not assimilated data). The results presented here suggest a model's imbalance adjustment time scale might be both smaller than, and proportional to, the chosen nudging time scale (Fig. 8).

The consequence of this result is quite important. If nudging tendencies were to be interpreted as total model or physics errors, then the errors so inferred would depend on the nudging time scale chosen. Still, systematic nudging tendencies represent a tendency of the model to push its state away from the target state. If the target state is considered "correct," then these tendencies still contain some information on model error, even if only qualitatively. However, nudging tendencies cannot be used to, for example, quantitatively identify forcing error profiles by a single parameterization known to dominate forcing in a particular profile.

The relevance of this result is significant as well. Nudging is a ubiquitous capability of numerical weather and climate models and is used widely in a variety of applications. While few have made use of the nudging tendencies themselves, an emerging application is to use methods to predict nudging tendencies of a model given its state in order to improve its predictive skill and reduce long-term biases. Watt-Meyer et al. (2021) and Bretherton et al. (2021) used machine learning to this, with some success, though they differed in the variables nudged and focused on. The results here do not invalidate such results, but suggest that they may depend not only on the model and resolution used, but also on the nudging time scale chosen.

The nudging method of data assimilation and model error quantification is likely the simplest in a spectrum of such methods. The results here are not expected to have any relevance to the initial tendency method or increment tendency methods of model error quantification (e.g. Klinker and Sardeshmukh (1992); Rodwell and Palmer (2007); Cavallo et al. (2016)). However, there may be some relevance to the incremental analysis update (IAU) method (Bloom et al., 1996; Rienecker et al., 2011), which applies analysis increment tendencies, held constant over an analysis window (e.g. 6 hours), in governing equations to "guide" a model's state along an analyzed trajectory. While there are similarities between the IAU and nudging methods, it is unclear at this point if a similar dependence of analysis increment tendencies on the analysis window chosen might exist.

Acknowledgments

All authors were supported either by the National Center for Atmospheric Research, which is a major facility sponsored by the National Science Foundation under Cooperative Agreement No. 1852977 or by a Climate Process Team grant from the National Science Foundation (NSF Grant Number(s) AGS-1916689). Simulations were performed with high-performance computing support from Cheyenne (doi:10.5065/D6RX99HX) provided by NCAR's Computational and Information Systems Laboratory, sponsored by the National Science Foundation. We also wanted to acknowledge interesting and helpful discussions with Judith Berner and Riwal Plougonven during the preparation of this manuscript.

References

Anthes, R. A. (1974). Data assimilation and initialization of hurricane prediction models. *Journal of Atmospheric Sciences*, *31*(3), 702 - 719. doi: 10.1175/1520-0469(1974)031⟨0702:DAAIOH⟩2.0.CO;2

Bao, J.-W., & Errico, R. M. (1997). An adjoint examination of a nudging method for data assimilation. *Monthly Weather Review*, *125*(6), 1355 - 1373. Retrieved from https://journals.ametsoc.org/view/journals/mwre/125/6/1520-0493_1997_125_1355_aaeoan_2.0.co_2.xml doi: 10.1175/1520-0493(1997)125⟨1355:AAEOAN⟩2.0.CO;2

Bloom, S. C., Takacs, L. L., da Silva, A. M., & Ledvina, D. (1996). Data assimilation using incremental analysis updates. *Monthly Weather Review*, *124*(6), 1256 - 1271. Retrieved from https://journals.ametsoc.org/view/journals/mwre/124/6/1520-0493_1996_124_1256_dauiau_2_0_co_2.xml doi: 10.1175/1520-0493(1996)124⟨1256:DAUIAU⟩2.0.CO;2

Blumen, W. (1972). Geostrophic adjustment. *Reviews of Geophysics*, *10*(2), 485-528. Retrieved from https://agupubs.onlinelibrary.wiley.com/doi/abs/10.1029/RG010i002p00485 doi: https://doi.org/10.1029/RG010i002p00485

Bretherton, C. S., Henn, B., Kwa, A., Brenowitz, N. D., Watt-Meyer, O., McGibbon, J., ... Harris, L. (2021). Correcting coarse-grid weather and climate models by machine learning from global storm-resolving simulations. *Submitted to JAMES*, 39. Retrieved from https://doi.org/10.1002/essoar.10507879.1 doi: 10.1002/essoar.10507879.1

Cavallo, S. M., Berner, J., & Snyder, C. (2016). Diagnosing model errors from time-averaged tendencies in the weather research and forecasting (wrf) model. *Monthly Weather Review*, *144*(2), 759 - 779. doi: 10.1175/MWR-D-15-0120.1

Charney, J., Halem, M., & Jastrow, R. (1969). Use of incomplete historical data to infer the present state of the atmosphere. *Journal of Atmospheric Sciences*, *26*(5), 1160 - 1163. Retrieved from https://journals.ametsoc.org/view/journals/atsc/26/5/1520-0469_1969_026_1160_uoihdt_2_0_co_2.xml doi: 10.1175/1520-0469(1969)026⟨1160:UOIHDT⟩2.0.CO;2

Davies, H. C., & Turner, R. E. (1977). Updating prediction models by dynamical relaxation: an examination of the technique. *Quarterly Journal of the Royal Meteorological Society*, *103*(436), 225-245. doi: https://doi.org/10.1002/qj.49710343602

Davis, N. A., Callaghan, P., Simpson, I. R., & Tilmes, S. (2021). Specified dynamics scheme impacts on wave-mean flow dynamics, convection, and tracer transport in cesm2 (waccm6). *Atmospheric Chemistry and Physics Discussions*, *2021*, 1–32. doi: 10.5194/acp-2021-169

Gettelman, A., Hannay, C., Bacmeister, J. T., Neale, R. B., Pendergrass, A. G., Danabasoglu, G., ... Mills, M. J. (2019). High climate sensitivity in the community earth system model version 2 (cesm2). *Geophysical Research Letters*, *46*(14), 8329-8337. Retrieved from https://agupubs.onlinelibrary.wiley.com/doi/abs/10.1029/2019GL083978 doi: https://doi.org/10.1029/2019GL083978

Hersbach, H., Bell, B., Berrisford, P., Hirahara, S., Horányi, A., Muñoz-Sabater, J., ... Thépaut, J.-N. (2020). The era5 global reanalysis. *Quarterly Journal of the Royal Meteorological Society*, *146*(730), 1999-2049. Retrieved from https://rmets.onlinelibrary.wiley.com/doi/abs/10.1002/qj.3803 doi: https://doi.org/10.1002/qj.3803

Jastrow, R., & Halem, M. (1970). Simulation studies related to garp. *Bulletin of the American Meteorological Society*, *51*(6), 490 - 514. Retrieved from https://journals.ametsoc.org/view/journals/bams/51/6/1520-0477-51_6_490.xml doi: 10.1175/1520-0477-51.6.490

Kao, C.-Y. J., & Yamada, T. (1988). Use of the captex data for evaluations of a long-range transport numerical model with a four-dimensional data as-

similation technique. *Monthly Weather Review*, *116*(2), 293 - 306. doi: 10.1175/1520-0493(1988)116⟨0293:UOTCDF⟩2.0.CO;2

Kistler, R. E. (1974). *A study of data assimilation techniques in an autobarotropic primitive equation channel model* (Unpublished doctoral dissertation). The Pennsylvania State University, State College, PA.

Klinker, E., & Sardeshmukh, P. D. (1992). The diagnosis of mechanical dissipation in the atmosphere from large-scale balance requirements. *Journal of Atmospheric Sciences*, *49*(7), 608 - 627. doi: 10.1175/1520-0469(1992)049⟨0608:TDOMDI⟩2.0.CO;2

Mapes, B. E., & Bacmeister, J. T. (2012). Diagnosis of tropical biases and the mjo from patterns in the merra analysis tendency fields. *Journal of Climate*, *25*(18), 6202 - 6214. Retrieved from `https://journals.ametsoc.org/view/journals/clim/25/18/jcli-d-11-00424.1.xml` doi: 10.1175/JCLI-D-11-00424.1

Plougonven, R., & Zhang, F. (2014). Internal gravity waves from atmospheric jets and fronts. *Reviews of Geophysics*, *52*(1), 33-76. Retrieved from `https://agupubs.onlinelibrary.wiley.com/doi/abs/10.1002/2012RG000419` doi: https://doi.org/10.1002/2012RG000419

Rienecker, M. M., Suarez, M. J., Gelaro, R., Todling, R., Bacmeister, J., Liu, E., ... Woollen, J. (2011). Merra: Nasa's modern-era retrospective analysis for research and applications. *Journal of Climate*, *24*(14), 3624 - 3648. Retrieved from `https://journals.ametsoc.org/view/journals/clim/24/14/jcli-d-11-00015.1.xml` doi: 10.1175/JCLI-D-11-00015.1

Rodwell, M. J., & Palmer, T. N. (2007). Using numerical weather prediction to assess climate models. *Quarterly Journal of the Royal Meteorological Society*, *133*(622), 129-146. doi: https://doi.org/10.1002/qj.23

Skamarock, W. C., Klemp, J. B., Dudhia, J., Gill, D. O., Barker, D. M., Duda, M. G., ... Powers, J. G. (2008). *A description of the Advanced Research WRF version 3* (Tech. Rep.). Boulder, Colorado: NCAR Tech. Note NCAR/TN-475+STR.

Stauffer, D. R., & Seaman, N. L. (1990). Use of four-dimensional data assimilation in a limited-area mesoscale model. part i: Experiments with synoptic-scale data. *Monthly Weather Review*, *118*(6), 1250 - 1277. doi: 10.1175/1520-0493(1990)118⟨1250:UOFDDA⟩2.0.CO;2

Watt-Meyer, O., Brenowitz, N. D., Clark, S. K., Henn, B., Kwa, A., McGibbon, J., ... Bretherton, C. S. (2021). Correcting weather and climate models by machine learning nudged historical simulations. *Geophysical Research Letters*, *48*(15). Retrieved from `https://agupubs.onlinelibrary.wiley.com/doi/abs/10.1029/2021GL092555` doi: https://doi.org/10.1029/2021GL092555